Effect of Reduction Atmosphere on Structure and Catalytic Performance of PtIn/Mg(Al)O/ZnO for Propane Dehydrogenation

Ming Zhang [1], Zhen Song [1], Mengquan Guo [1], Xiangxiang Li [1], Yanjun Lin [2,*] and Lihong Zhang [1,*]

[1] Department of Catalysis Science and Technology and Tianjin Key Laboratory of Applied Catalysis Science Technology, School of Chemical Engineering and Technology, Tianjin University, Tianjin 300350, China; minne_zhang@hotmail.com (M.Z.); songzhens12345@163.com (Z.S.); Guo_mengquan@163.com (M.G.); lixx_37@tju.edu.cn (X.L.)

[2] State Key Laboratory of Chemical Resource Engineering, Beijing University of Chemical Technology, Beijing 100029, China

* Correspondence: linyj@mail.buct.edu.cn (Y.L.); zlh_224@163.com (L.Z.); Tel.: +86-136-4138-6787 (Y.L.); +86-150-2225-5828 (L.Z.)

Abstract: The effect of reduction atmospheres, H_2/N_2, $C_3H_8/H_2/N_2$, C_3H_8 and CO, on the structure and propane direct dehydrogenation performance of PtIn/Mg(Al)O/ZnO catalyst derived from ZnO-supported PtIn-hydrotalcite was studied. The physicochemical properties of the as-prepared and used catalytic system were characterized by various characterization methods. The results show that the dehydrogenation performance, especially the stability of the PtIn/Mg(Al)O/ZnO catalyst, was significantly improved along with the change in reduction atmosphere. The highest catalytic activity (51% of propane conversion and 97% propylene selectivity), resistance toward coke deposition, and stability for more than 30 h were achieved with the H_2/N_2-reduced catalyst. The optimal dehydrogenation performance and coke resistance are mainly related to the high Pt dispersion and In^0/In^{3+} molar ratio, strong Pt–In interaction and small metal particle size, depending on the nature of the reduction atmospheres. The reconstruction of meixnerite favors the stability and coke resistance to some extent.

Keywords: propane dehydrogenation; reduction atmosphere; coke deposition; meixnerite; PtIn/Mg(Al)O/ZnO

1. Introduction

In recent years, the dehydrogenation of low alkanes to the corresponding alkenes has drawn great attention from the world, due to their extensive utilization as raw materials and a versatile class of intermediates in the polymer industry. In this context, it is particularly important to dehydrogenate propane to propylene (PDH) because of the rapidly growing demand for propylene in the production of propylene oxide, acrylonitrile and polypropylene [1–3]. The preparation and structure studies of catalysts with high efficiency propylene yield become the key point of PDH.

At present, Al-Cu catalysts, Co/SiO$_2$ catalysts, Ce-based catalysts, etc., are mainly novel catalysts developed by researchers [4–6]. However, Pt-based catalysts are still regarded as the most effective catalysts for PDH process, especially when working with a promoter, such as In, Sn, Ga or Zn, which can further improve propylene selectivity [1,7–10].

The support materials, Al$_2$O$_3$ [11], SiO$_2$ [6], ZrO$_2$ [12,13] and zeolite [3,14], can also affect catalytic performance on account of the significant differences in textural properties. Especially, the Mg(Al)O

oxides obtained by calcining hydrotalcite compounds (HT) have been studied extensively during the past years, owing to their suitable acid–base properties, high thermal stability, large surface area and memory effect [15–23]. Simultaneously, the stability of support plays an important role in reactions. Many works have been tried to stabilize the HT-based catalysts by combining with graphene networks [17,24], growing on metal (Al, Ni) or alloy substrates [25,26] and loading on oxide materials (γ-Al$_2$O$_3$, ZnO, SnO$_2$) [27–29].

It is well known that the activity of PDH is susceptible to many factors. Some researchers have studied the preparation conditions of Mg(Al)O support, such as Mg/Al molar ratio, pH value, and calcination temperature of the HT precursor [19,21,30,31]. Others have discussed the effect of loading methods and precursors of Pt on PDH [32,33]. Still others investigated the dehydrogenation reaction conditions (temperature, co-feed gas), In/Pt molar ratio and formation of PtIn alloy [15,34,35]. Most of the factors have been studied in detail. However, this does not seem to be the case for the reduction atmosphere of Mg(Al)O-supported Pt-based catalysts. Thus, the relationships between reduction atmosphere and catalysts' performance deserve to be studied.

In this paper, the influence of reduction atmospheres on the structural properties and catalytic performance of the PtIn/Mg(Al)O/ZnO (PtIn/MAZ) catalytic system was studied. ZnO was employed as the support for PtIn/Mg(Al)O catalytic system on account of its good stability. On this basis, ZnO-supported HT was prepared by the hydrothermal method, then In and Pt elements were introduced into the HT layer by sequential impregnation-induced reconstruction. H$_2$/N$_2$, C$_3$H$_8$/H$_2$/N$_2$, C$_3$H$_8$ and CO were selected as the reduction atmospheres, which are commonly used or produced in the reaction and likely to affect the catalytic performance. The precursors, calcined samples and reduced catalytic system were characterized by X-ray diffraction (XRD), transmission electron microscopy (TEM), X-ray photoelectron spectroscopy (XPS), thermogravimetric (TG) and CO chemisorption. The PDH reaction was performed at 600 °C and atmospheric pressure with the gas mixture of C$_3$H$_8$, H$_2$ and N$_2$.

2. Results and Discussion

2.1. Catalytic Activity

A series of PtIn/MAZ reduced with different atmospheres (H$_2$/N$_2$, C$_3$H$_8$/H$_2$/N$_2$, C$_3$H$_8$ and CO) at 600 °C for 2.5 h were evaluated in PDH reaction, and their propane conversions and propylene and by-product selectivities as a function of time on stream are shown in Figure 1. During the 17 h on stream, propane conversion and propylene selectivity showed an obvious improvement with the reduction atmosphere changing from CO to C$_3$H$_8$ and to C$_3$H$_8$/H$_2$/N$_2$. This should arise from the different surface chemical states of the active metal species. An "induction period" appeared for all samples, especially the activity of the CO-reduced sample, which had a long induction period. This can be explained by the in-situ creation of the active metal species [11]. Additionally, it was found that there nearly no cracking products were formed on the samples reduced with C$_3$H$_8$ and C$_3$H$_8$/H$_2$/N$_2$ during the period of ~ 17 h. However, the CO-reduced sample had more cracking products at the initial stage and presented a decreasing tendency with time on stream, together with ascending propylene selectivity. This agrees with the phenomenon that CO pre-reduction can result in violent cracking at the initial stage [36,37]. Furthermore, the replacement of C$_3$H$_8$/H$_2$/N$_2$ by H$_2$/N$_2$ slightly decreased the conversion but enhanced the initial activity and catalytic stability. Nevertheless, there were no obvious difference between their propylene and by-product selectivities during the reaction lasting for 17 h.
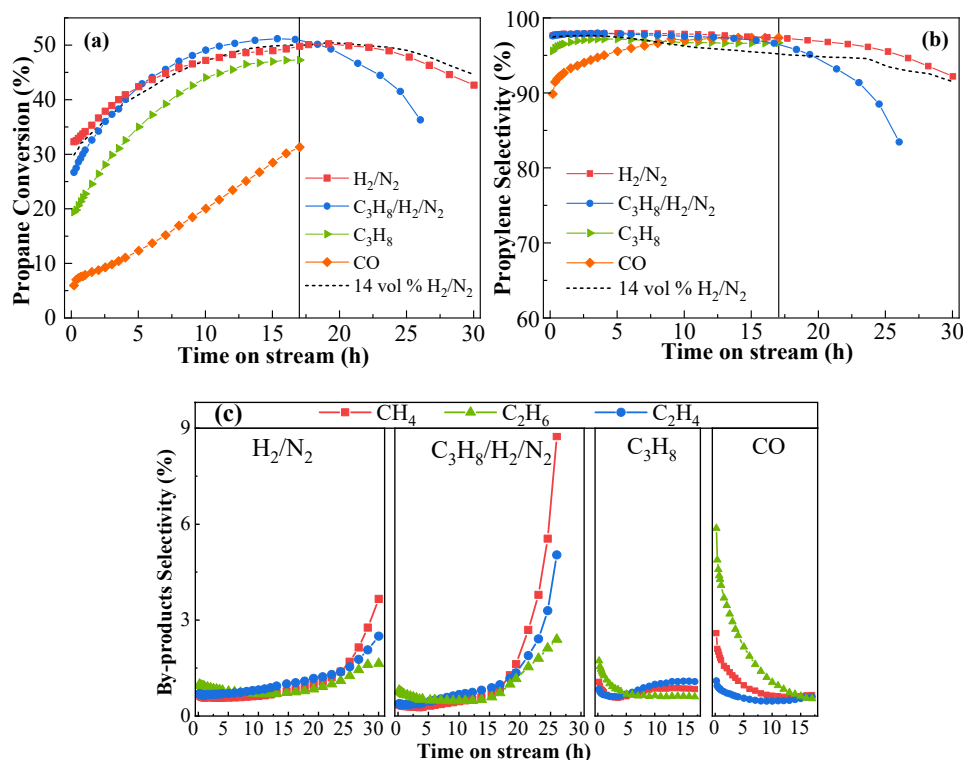
Figure 1. Catalytic performances of PtIn/MAZ catalytic system reduced with different atmospheres: (**a**) propane conversion; (**b**) propylene selectivity; (**c**) by-product selectivity (reduction conditions: T = 600 °C, t = 2.5 h; reaction conditions: T = 600 °C, weight hourly space velocity (WSHV) = 3 h^{-1}, atmospheric pressure in the gas mixture of C_3H_8:H_2:N_2 molar ratio = 8:7:35; reaction time: 30 h for H_2/N_2 and 14 vol % H_2/N_2 reduced catalyst, 26 h for $C_3H_8/H_2/N_2$-reduced catalyst, 17 h for C_3H_8 and CO-reduced catalyst).

Since the activities of $C_3H_8/H_2/N_2$- and H_2/N_2-reduced catalytic systems were much higher than those of the others, the reaction time was extended to 30 h to compare the stability of the $C_3H_8/H_2/N_2$- and H_2/N_2-reduced catalytic systems. When the reaction time was prolonged, some distinct and significant differences could be found between them. With a reaction of 30 h, the propane conversion and propylene selectivity of H_2/N_2-reduced samples were maintained at more than 45% and 92% and the by-product selectivity was less than 4%, respectively. However, the $C_3H_8/H_2/N_2$-reduced catalyst showed a rapid decrease of propane conversion and propylene selectivity after 18 h along with the increase of cracking products. In order to evaluate the effect of H_2 content, the 14 vol% H_2/N_2 with the same H_2 content as $C_3H_8/H_2/N_2$ was also adopted for the comparison. It is noticeable that the propane conversion and propylene selectivity of the 14 vol% H_2/N_2-reduced sample was similar to that of the H_2/N_2-reduced one. This indicates that the reducibility of H_2/N_2 is quite similar to that of 14 vol% H_2/N_2 under this reduction temperature. Therefore, the different performance between H_2/N_2 and $C_3H_8/H_2/N_2$ is arising from the presence of C_3H_8 in $C_3H_8/H_2/N_2$, which makes the $C_3H_8/H_2/N_2$-reduced sample rapidly deactivate along with the increase of cracking products. Meanwhile, the H_2/N_2-reduced sample had effective catalytic stability and crack resistance.

2.2. Texture and Structure of Reduced Catalystic Systems

2.2.1. XRD

According to the XRD patterns of precursors and calcined samples obtained with different preparation processes in Figure S1, it could be confirmed that the HT phase can be formed on the ZnO precursor (hydrozincite phase, JCPDS file No. 19-1458); even the ZnO-supported PtIn-HT can be acquired by impregnation-induced reconstruction. After calcination, only MgO phases (JCPDS file

No. 87-0651) could be indexed on ZnO (JCPDS file No. 75-0576). The Al_2O_3 diffraction peaks could not be found, as it is retained and located in interstitial sites in the MgO framework after calcination [38]. There were no diffraction peaks of Pt-(In-)-based compounds, as a result of their low concentration or uniform distribution [38].

In order to evaluate the crystalline phase of the reduced PtIn/MAZ catalytic system, XRD characterization was conducted, and the results are shown in Figure 2. It can be noted that the XRD patterns of all samples show the same crystalline diffraction peaks. The main crystalline phases were ZnO and MgO and the peaks were same with those of calcined ones (Figure S1B). This means the change in reduction atmosphere did not cause the obvious change of crystal phases. The diffraction peaks of Pt(In)-species still could not be recognized for the reduced PtIn/MAZ catalytic system. This is owing to the small and uniform distribution of Pt(In) species on the support or the low concentration [19].
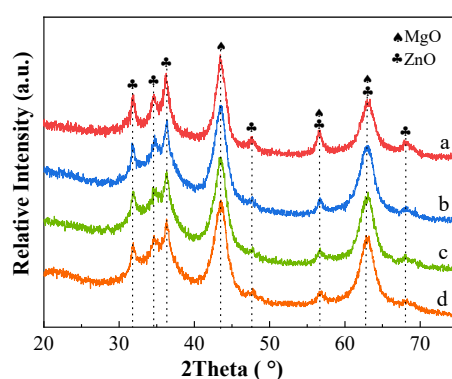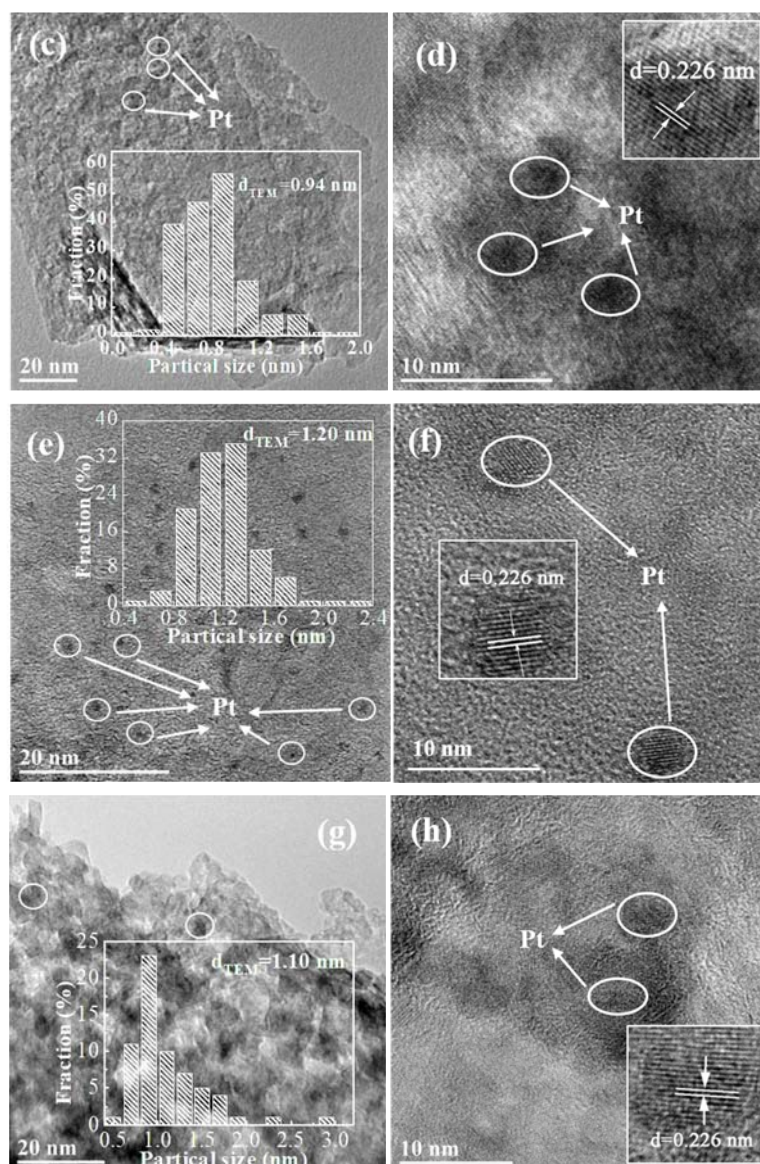

Figure 2. XRD patterns of PtIn/MAZ catalytic systems reduced with different atmospheres: (a) H_2/N_2; (b) $C_3H_8/H_2/N_2$; (c) C_3H_8; (d) CO (reduction conditions: T = 600 °C, t = 2.5 h).

2.2.2. TEM

The morphology, phase composition and particle size distribution (PSD) of the reduced catalytic system are given in Figure 3. Although it is difficult to distinguish the diffraction of metallic phases from the XRD patterns in Figure 1, the metallic Pt (111) nanoparticles (NPs) can be recognized in the HR-TEM depending on the lattice spacing of 0.226 nm. Meanwhile, PtIn alloy (d = 0.208 nm) can be detected on the H_2/N_2-reduced sample. From the PSD of all samples, the average particle size of metals was in the range from 0.85–1.20 nm. The small metal NPs can be related to the PtIn-HT reconstruction, as described in Figure S1. Moreover, the average metal particle sizes of H_2/N_2- and $C_3H_8/H_2/N_2$-reduced samples are smaller than that of C_3H_8- and CO-reduced ones. This indicates that the H_2-containing reduction gas is more efficient to obtain smaller metallic particles. The smaller metal particles are more active for propane dehydrogenation performance and beneficial to resist the coke deposition [39].
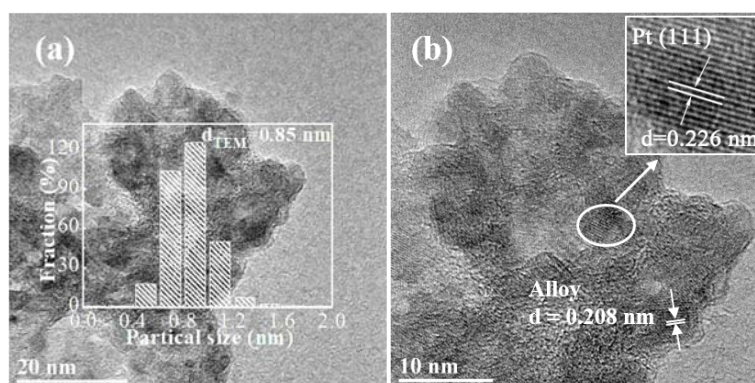

Figure 3. *Cont.*

Figure 3. TEM images, HR-TEM and the statistics of PSD in the insets of PtIn/MAZ catalytic system reduced with different atmospheres: (**a**,**b**) H_2/N_2; (**c**,**d**) $C_3H_8/H_2/N_2$; (**e**,**f**) C_3H_8; (**g**,**h**) CO (reduction conditions: T = 600 °C, t = 2.5 h).

2.2.3. XPS

The chemical states of In species over the reduced catalytic system were determined by XPS measurements. The Pt 4f spectra is not shown here due to the difficulty of distinguishing it from the Al 2p peak [40]. The XPS spectra of the $In3d_{5/2}$ region are shown in Figure 4, and the semi-quantitative results of the corresponding spectra are summarized in Table 1. The $In3d_{5/2}$ level can be split into two peaks at ~444.1 eV and ~445.2 eV, which represent In^0 (metallic In or PtIn alloy) and In^{3+}, respectively. As shown in Table 1, the In^0/In^{3+} molar ratios for H_2/N_2-, $C_3H_8/H_2/N_2$-, C_3H_8- and CO-reduced samples were 2.50, 1.22, 0.59 and 0.78, respectively. According to the downward trend of the In^0/In^{3+} molar ratio from H_2/N_2 to $C_3H_8/H_2/N_2$ and to C_3H_8, it is assumed that the presence of C_3H_8 can impede the formation of zero-valence In. The deduction is based on the similar reducibility between H_2/N_2 and 14 vol % H_2/N_2, which has been proved by the corresponding catalytic performance in Figure 1. In view of this, the In^0/In^{3+} molar ratio in the $C_3H_8/H_2/N_2$-reduced sample should be equal to or higher than that of the H_2/N_2-reduced one, due to the co-existence of H_2 and C_3H_8. The opposite

results indicate that the C_3H_8 must impede the reduction of In^{3+} ions. In this way, it is not difficult to understand why the In^0/In^{3+} molar ratio of CO-reduced sample was higher than C_3H_8-reduced one. The In^0/In^{3+} molar ratio of the CO-reduced sample was lower than that of H_2-containing reduced sample, indicating that the reduction ability of CO to In^{3+} was weaker than that of H_2. The In^0 has been proved to promote the transfer of coke from the active site to the support and the stabilization of the active metal species [40,41]. Meanwhile, the presence of C_3H_8 leads to a decrease of In^0, thus the propylene selectivity of the H_2/N_2-, $C_3H_8/H_2/N_2$- and C_3H_8-reduced catalytic systems decreases accordingly (see Figure 1).
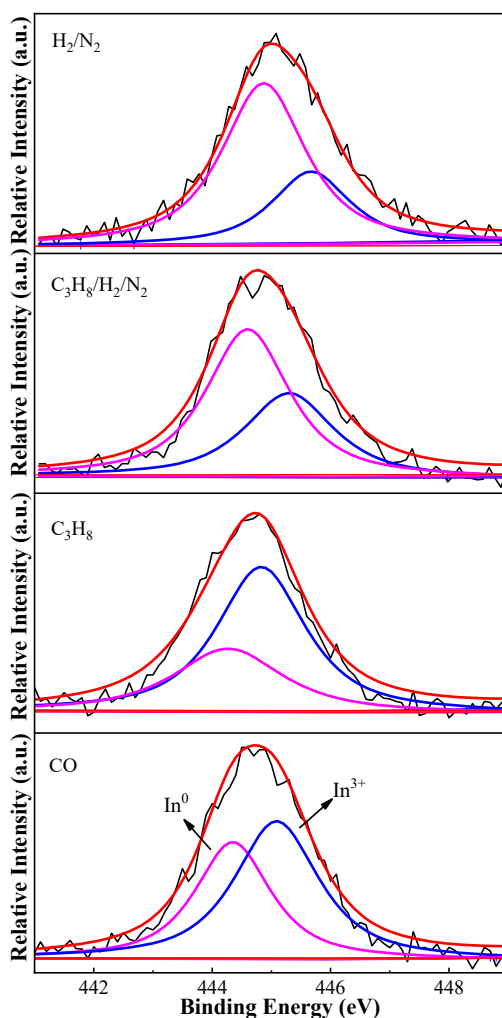
Figure 4. $In3d_{5/2}$ XPS spectra of a PtIn/MAZ catalytic system reduced with different atmospheres (reduction conditions: T = 600 °C, t = 2.5 h).

Table 1. XPS results and Pt dispersion of a PtIn/MAZ catalytic system reduced with different atmospheres [a] (reduction conditions: T = 600 °C, t = 2.5 h).

Reduction Atmosphere	Binding Energy (eV)		In^0/In^{3+} Molar Ratio [b]	Pt Dispersion [c]
	In^0	In^{3+}		
H_2/N_2	444.9	445.7	2.50	48%
$C_3H_8/H_2/N_2$	444.5	445.2	1.22	34%
C_3H_8	444.3	444.8	0.59	—
CO	444.4	445.1	0.78	—

[a] All samples were protected with Ar from oxidation prior to test. [b] Calculated from the fitting peak area results of $In3d_{5/2}$ XPS spectra. [c] Computed from the CO chemisorption results.

The binding energy (BE) value of In^0 presented a slightly decreasing trend in accordance with the order of H_2/N_2-, $C_3H_8/H_2/N_2$-, CO- and C_3H_8-reduced samples, signifying the weakening Pt–In interaction and transfer of electrons from metallic In to Pt species [22]. The electron-rich Pt sites are beneficial to hindering the adsorption of alkenes on active sites, consequently decreasing the likelihood of hydrogenolysis and coking [42].

The Pt dispersion of H_2/N_2- and $C_3H_8/H_2/N_2$-reduced samples was evaluated by CO chemisorption due to their far better propane dehydrogenation performance than the other two samples. According to the results in Table 1, the 48% dispersion of H_2/N_2 reduced sample is obviously higher than the 34% dispersion of the $C_3H_8/H_2/N_2$-reduced one. This indicates that the H_2/N_2-reduced catalyst had a higher utilization of Pt. Combined with the high In^0/In^{3+} molar ratio and the formation of PtIn alloy in the H_2/N_2-reduced sample, it can be deduced that the Pt–In synergistic effect, high Pt dispersion and large In^0 content result in good activity and high stability to some degree.

2.3. Analysis of The Used Catalytic System

2.3.1. XRD

Figure 5 shows the XRD patterns of the used catalytic system. Compared with the reduced catalytic system, the characteristic diffraction peaks of graphite (JCPDS file No. 75-1621) appear at 2θ of ca. 26° and 44°. The peak intensity at 2θ of 26° cuts down progressively following the order of the catalyst reduced with C_3H_8, $C_3H_8/H_2/N_2$, CO and H_2/N_2, which is correlated with the crystallinity of graphite. It can be declared that the heavily condensed coke species are more difficult to form on the H_2/N_2-reduced catalyst than others. At the same time, this also means that the H_2/N_2-reduced catalyst is easy to regenerate via oxidation in air [43]. In addition, the Pt and In species still cannot be distinguished, indicating that the metal species are quite stable and highly dispersed on the surface of PtIn/MAZ.
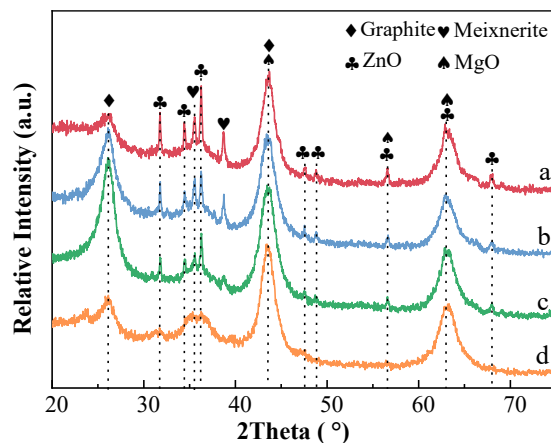
Figure 5. XRD patterns of the used PtIn/MAZ catalytic system reduced with different atmospheres: (a) H_2/N_2; (b) $C_3H_8/H_2/N_2$; (c) C_3H_8; (d) CO (reduction conditions: T = 600 °C, t = 2.5 h; reaction conditions: T = 600 °C, WSHV = 3 h^{-1}, atmospheric pressure in the gas mixture of $C_3H_8:H_2:N_2$ molar ratio = 8:7:35 for 17 h).

It is interesting to notice that the diffraction peaks of meixnerite (JCPDS file No. 38-0478) appeared at 2θ of 35° and 39° in the used catalytic system, instead of the reduced ones reported in [43]. This arises from the high dispersion or low content of meixnerite. On the other hand, the intensity of the corresponding diffraction peaks decreased gradually with the order of H_2/N_2, $C_3H_8/H_2/N_2$, C_3H_8 and CO-reduced sample, and even completely disappeared for PtIn/MAZ reduced with CO.

The formation of meixnerite can be explained by the reconstruction of the calcined HT under the humidified conditions [41,44–46]. As we all know, the calcination can cause H_2O and -OH removal from the structure [47,48]. However some highly temperature-stable $M-OH_2$ can be formed on the

surface of PtIn/MAZ after reduction with H-containing gas, due to the strong water affinity of calcined HT structure [45]. It is just that the PDH reaction further provides the sufficient -OH$_2$ concentration level and exposure time on the surface of calcined HT, which makes the calcined HT reconstruct into meixnerite. Therefore, the differences of meixnerite peak intensity among the H$_2$/N$_2$-, C$_3$H$_8$/H$_2$/N$_2$- and C$_3$H$_8$-reduced samples can arise from the different levels of -OH$_2$, depending on the reducibility of these atmospheres. As a result, the strong diffraction peaks of meixnerite can be obtained by the H$_2$/N$_2$-reduced sample. The complete disappearance of meixnerite for the CO-reduced sample may have been induced by the formation of bicarbonate species, together with the consumption of oxygen, resulting in no conditions for the formation of meixnerite [36]. As a kind of HT with an interlayer -OH anion, the high crystallinity meixnerite may be helpful to keep the high dispersion and uniform distribution of surface metal active sites during reaction. As a result, the good stability of the H$_2$/N$_2$-reduced sample can arise from the formation of meixnerite to a certain extent [17].

Additionally, it has been proved that the meixnerite has Brønsted basicity [49], which is different from the Lewis basicity of calcined HT. Thus, the formation of meixnerite can adjust the acid–base properties of the catalyst and improve its coke resistance [50,51]. However, it is difficult to evaluate the acid–base properties by conventional methods because of the influence of deposited coke on the formed meixnerite [50,51]. As compared with the diffraction strength of meixnerite, the only direct evidence is that the diffraction strength of graphite and the amount of deposited coke (see TG analysis below) show an opposite trend in accordance with the order from H$_2$/N$_2$- to C$_3$H$_8$/H$_2$/N$_2$- and C$_3$H$_8$-reduced catalysts.

2.3.2. TEM

After a reaction of 17 h, the TEM images and the PSD statistics of the used catalytic system reduced with different atmospheres are shown in Figure 6. It was found that the range of PSD became wider, but the average metal particle size only showed a slight increase compared with the corresponding reduced catalytic system. The slight aggregation of metal particles agrees with the fact that the reaction is not in the deactivation stage (Figure 1). It is worth noting that the metal sintering degree of the C$_3$H$_8$/H$_2$/N$_2$-reduced sample was higher than that of the H$_2$/N$_2$-reduced one, although they had similar catalytic performance during a reaction of 17 h. Therefore, this can be used to explain the stable catalytic performance of the H$_2$/N$_2$-reduced catalyst and the rapid decline in reactivity of the C$_3$H$_8$/H$_2$/N$_2$-reduced sample after a reaction of 17 h. This is attributable to the initial smaller metal particles and high Pt dispersion of the H$_2$/N$_2$-reduced catalyst. Meanwhile, it indicates strong Pt–In or Pt–support interaction, which results in the superior stability of Pt during the PDH reaction [40]. Coke deposits can be found on the support surface of the used catalytic system instead of the active site, which means that the formed coke should be shifted to the surface of support before a reaction of 17 h [40].
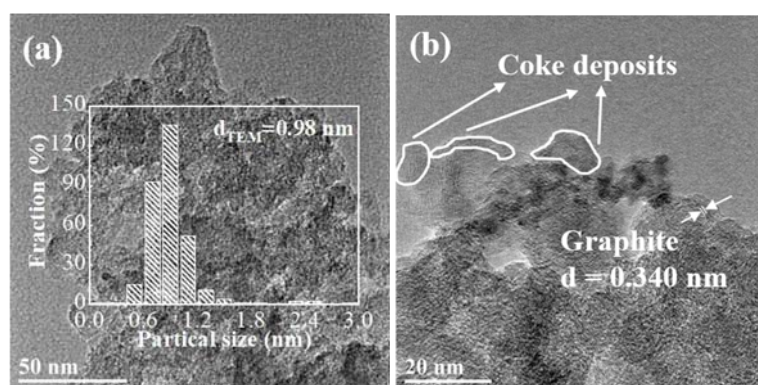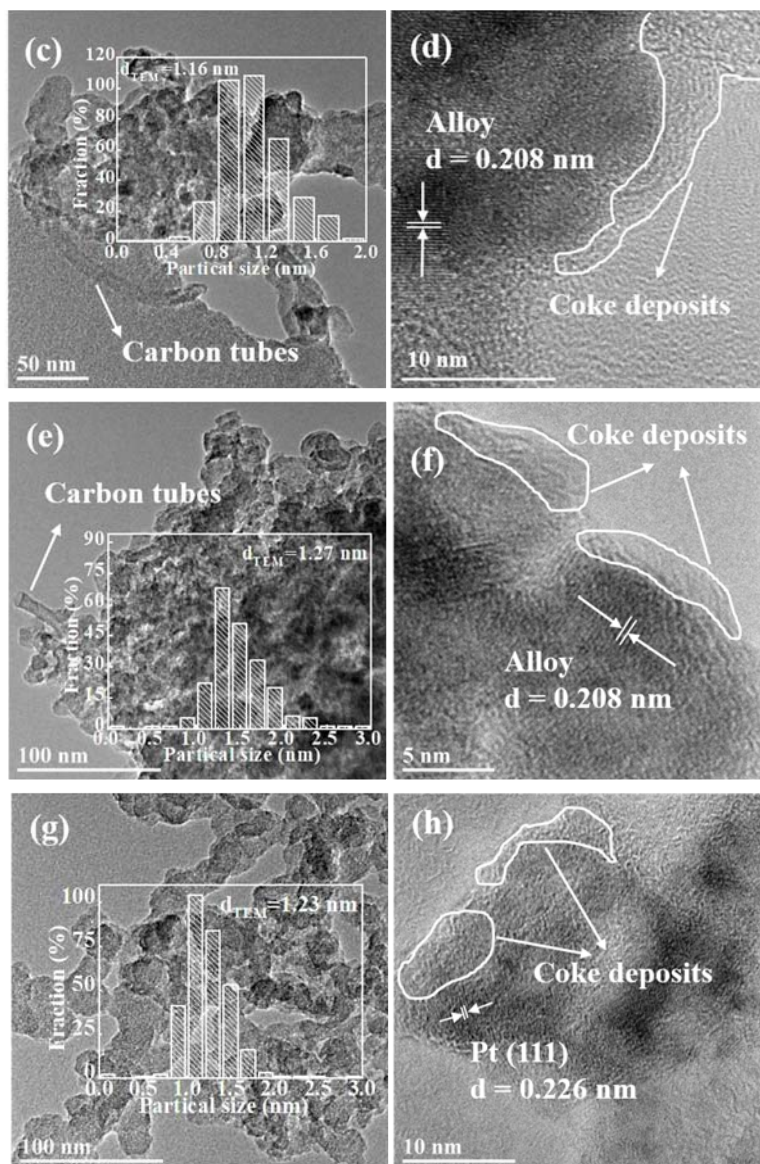

Figure 6. *Cont.*

Figure 6. TEM images and the statistics of PSD in the insets of the used PtIn/MAZ catalytic system reduced with different atmospheres: (**a**,**b**) H_2/N_2; (**c**,**d**) $C_3H_8/H_2/N_2$; (**e**,**f**) C_3H_8; (**g**,**h**) CO (reduction conditions: T = 600 °C, t = 2.5 h; reaction conditions: T = 600 °C, WSHV = 3 h^{-1}, atmospheric pressure in the gas mixture of C_3H_8:H_2:N_2 molar ratio = 8:7:35 for 17 h).

2.3.3. TG

In order to evaluate the amounts of deposited coke on the used catalytic system, the TG test was adopted, and the results are shown in Figure 7. The total deposited coke content of the catalyst pre-reduced with H_2/N_2 was only 27 wt %, and lower than the others, which coincided with its high propylene selectivity (see Figure 1). The lowest coke formation on H_2/N_2-reduced catalyst should be related to the small metal particle size, strong Pt–In interaction and suitable acid–base properties caused by the formation of meixnerite. Meanwhile, the more In^0 species also can promote the transfer of coke deposition from the active sites to the support, maintaining the stability of active metal species, ensuring the selectivity of propylene and reducing the occurrence of cracking. The pre-reduction with $C_3H_8/H_2/N_2$ and C_3H_8 made the deposited coke content increase to ca. 50 wt %. The severe coke deposition has been proposed to explain the fast loss of activity of the $C_3H_8/H_2/N_2$-reduced sample [47]. This is thought to be related to their wide PSD [47]. The mass loss of CO-reduced catalyst is lower than the $C_3H_8/H_2/N_2$- and C_3H_8-reduced one is, because it is far below propane conversion than them.
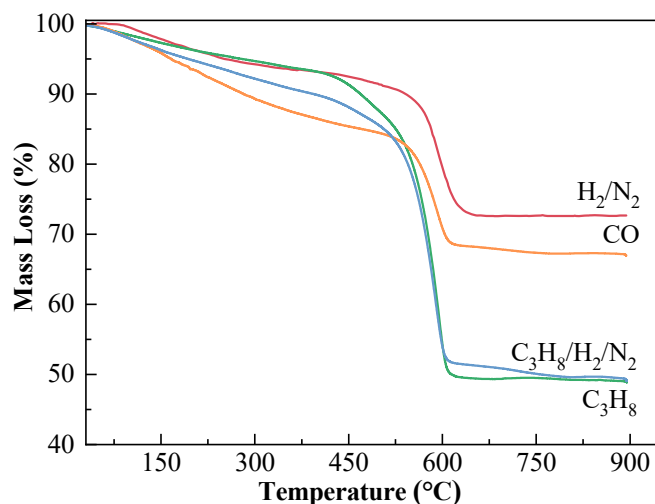
Figure 7. TG curves of the used PtIn/MAZ catalytic system reduced with different atmospheres (reduction conditions: T = 600 °C, t = 2.5 h; reaction conditions: T = 600 °C, WSHV = 3 h^{-1}, atmospheric pressure in the gas mixture of C_3H_8:H_2:N_2 molar ratio = 8:7:35 for 17 h).

In comparison with the state-of-the-art Pt-based catalysts in the literature (Table S1), the PtIn/MAZ catalytic system obtained in this work possesses much higher catalytic performance and attractive stability.

3. Materials and Methods

3.1. Materials

The reagents for the preparation of catalyst were analytical grade chemicals. $Zn(NO_3)_2 \cdot 6H_2O$, $Mg(NO_3)_2 \cdot 6H_2O$, $Al(NO_3)_3 \cdot 9H_2O$ and urea were purchased from Tianjin Fuchen Chemical Regents Factory (Tianjin, China). $H_2PtCl_6 \cdot 6H_2O$ was purchased from Tianjin Mascot Chemical Co. Ltd (Tianjin, China). $InNO_3 \cdot xH_2O$ was purchased from Aladdin Industrial corporation (Shanghai, China).

3.2. Preparation of ZnO Precursor

The ZnO precursor was prepared by the hydrothermal method. Briefly, 0.004 mol of $Zn(NO_3)_2 \cdot 6H_2O$ and 0.083 mol of urea was fully dissolved in 65 mL deionized water, then moved to a Teflon-lined stainless steel autoclave at 100 °C for 20 h. After cooling to room temperature, the products were filtrated and washed with deionized water till neutrality, then dried at 100 °C overnight to obtain the ZnO precursor.

3.3. Preparation of MAZ Support

The Mg(Al)O/ZnO (MAZ) precursor was prepared by the hydrothermal method. The molar ratio of Mg/Al is 2. Firstly, 0.1 g of ZnO precursor was introduced in 65 mL of a mixed solution, including 0.003 mol of $Mg(NO_3)_2 \cdot 6H_2O$, 0.0015 mol of $Al(NO_3)_3 \cdot 9H_2O$ and 0.1 mol of urea under vigorous stirring. After hydrothermal treatment in a Teflon-lined stainless-steel autoclave at 100 °C for 20 h, the mixture was cooled to room temperature. Next, the slurry was filtrated and washed with deionized water till to neutrality, then dried at 100 °C overnight. Finally, the corresponding MAZ support was obtained by calcining the precursor at 600 °C for 4 h in a muffle furnace with a heating rate of 5 °C min^{-1}.

3.4. Preparation and Reduction of PtIn/MAZ

The PtIn/MAZ precursor was synthesized via successive incipient wetness impregnation method. Firstly, the MAZ support was impregnated with an $InNO_3 \cdot xH_2O$ aqueous solution at room temperature

for 6 h and dried at 120 °C for 12 h to acquire the In/MAZ precursor. After calcination at 550 °C for 4 h, the In-based calcined product was obtained and labelled as In/MAZ. Next, the same processes were performed on In/MAZ by impregnating with an $H_2PtCl_6 \cdot 6H_2O$ aqueous solution to acquire the PtIn/MAZ precursor.

The calcined product PtIn/MAZ was obtained by calcining the corresponding precursor at 550 °C for 4 h with a heating rate of 5 °C min^{-1} [19,41]. To be consistent with previous research [22], the loading amounts of Pt and In were 0.5 wt % and 1.4 wt %, respectively.

Before the PDH reaction, PtIn/MAZ was reduced with different atmospheres. The reduction atmospheres of H_2/N_2 (5 vol % H_2), $C_3H_8/H_2/N_2$ (16 vol % C_3H_8 and 14 vol % H_2), C_3H_8 and CO were used to reduce PtIn/MAZ at 600 °C for 2.5 h respectively. In order to compare with H_2/N_2 (5 vol % H_2) and $C_3H_8/H_2/N_2$ (16 vol % C_3H_8 and 14 vol % H_2), the reduction gas of 14 vol % H_2/N_2 was also evaluated in the PDH reaction.

3.5. Catalyst Characterizations

The X-ray diffraction (XRD) patterns were recorded on a Bruker D8-Focus X-ray diffractometer (BRUKER AXS GMBH, Karlsruhe, Germany) equipped with Cu Kα radiation (λ = 0.15418 nm). The samples were scanned from the 2θ value of 20°–75°, with a scanning speed of 8°·min^{-1}. The X-ray tube was manipulated at 40 kV and 40 mA.

The transmission electron microscopy (TEM) images were taken with a JEM-2100F field-emission transmission electron microscope (JEOL, Tokyo, Japan) operated at 200 kV. The as-synthesized samples were dispersed, sonicated in ethanol, and dropped on carbon-film coated copper grids.

X-ray photoelectron spectroscopy (XPS) was carried out on a Perkin-Elmer PHI 5000C ESCA (PerkinElmer, Waltham, MA, USA) using Al Kα radiation. Prior to the analysis, the samples were reduced under different atmospheres (30 mL min^{-1}) at 600 °C for 2.5 h, and the binding energies were calibrated using the C1s peak at 284.8 eV as an internal standard. The whole process from reduction to test was strictly protected with Ar, which can avoid the re-oxidation of In^0.

Thermogravimetric (TG) analysis was carried out with a DTG-50/50H thermal analyzer (PerkinElmer, Waltham, MA, USA) to determine the quantity of coke on the used catalyst, and the TG curves were recorded from room temperature to 900 °C at an increasing rate of 10 °C min^{-1}.

Dispersion of metals was determined by CO chemisorption, CO chemisorption was conducted on AutoChem II 2920 analyzer (Micromeritics, Norcross, GA, USA). For a fresh catalyst, 100 mg of sample was pre-reduced with different atmospheres at 600 °C for 2.5 h and then purged with Ar flow at 300 °C for 0.5 h. CO chemisorption was carried out at 30 °C by injecting 50 μL CO every 3 min until the peak area became stable. The adsorption capacity of CO is calculated by the following Equation.

$$\text{CO uptakes (μmol g}^{-1}\text{}_{cat}) = n \times (A - B) \times 50 \times 10/A \times 22.4 \tag{1}$$

where *n* stands for the number of chemical adsorption peaks, *A* represents the average value of the peak area when the peak area remains constant, and *B* stands for the total area of the chemical adsorption peaks.

3.6. Catalytic Measurements

The PDH reactions were carried out in a fixed-bed quartz reactor with an 8-mm inner diameter. A quantity of 0.4 g of fresh catalyst (particle size of 40 to 60 meshes) was placed into the center of quartz tube reactor and reduced with different reduction atmospheres, as described in Section 2.3. Afterwards, the mixed gas, including C_3H_8, H_2 and N_2 (C_3H_8:H_2:N_2 molar ratio = 8:7:35), was fed at a rate of 62 mL min^{-1} into the reactor. The PDH reactions were performed at atmospheric pressure, 600 °C and a weight hourly space velocity (WHSV) of 3 h^{-1}, which was generally used in relevant studies [21,52,53]. A gas chromatograph equipped with an FID detector and Al_2O_3 column was

employed to analyze the gas compositions. The propane conversion and propylene selectivity were calculated by the following Equations:

$$\text{Conversion}(\%) = \frac{\text{propane, in - propane, out}}{\text{propane, in}} \times 100 \qquad (2)$$

$$\text{Selectivity}(\%) = \frac{\text{propylene, out}}{\text{propane, in - propane, out}} \times 100 \qquad (3)$$

4. Conclusions

A catalyst, PtIn/Mg(Al)O/ZnO, can be obtained by calcination and reduction of ZnO-supported PtIn-HT. The reduction atmosphere has a profound influence on the physicochemical nature and catalytic performance of the PtIn/Mg(Al)O/ZnO catalyst. The propane conversion and propylene selectivity of the catalyst reduced with H_2/N_2 can reach 51% and 97%, respectively, and even stabilize at 45% and 92% after running for 30 h. This is mainly attributable to its high Pt dispersion and In^0/In^{3+} molar ratio, strong Pt–In interaction and small metal particle size, which also result in a low content of coke deposits on the surface of the H_2/N_2-reduced catalyst. In addition, meixnerite can be formed after the reaction, and the crystallinity is influenced by the reduction atmosphere. At the same time, the formation of the high-crystallinity meixnerite can re-disperse the metal active sites and adjust the acid–base properties of the catalyst, thus improving the stability and coke resistance to some extent.

References

1.　Sun, P.; Siddiqi, G.; Chi, M.; Bell, A.T. Synthesis and characterization of a new catalyst Pt/Mg(Ga)(Al)O for alkane dehydrogenation. *J. Catal.* **2010**, *274*, 192–199. [CrossRef]

2.　Sahebdelfar, S.; Bijani, P.M.; Saeedizad, M.; Zangeneh, F.T.; Ganji, K. Modeling of adiabatic moving-bed reactor for dehydrogenation of isobutane to isobutene. *Appl. Catal. A* **2011**, *395*, 107–113. [CrossRef]

3.　Caeiro, G.; Carvalho, R.H.; Wang, X.; Lemos, M.A.N.D.; Lemos, F.; Guisnet, M.; Ramôa Ribeiro, F. Activation of C2-C4 alkanes over acid and bifunctional zeolite catalysts. *J. Mol. Catal. A Chem.* **2006**, *255*, 131–158. [CrossRef]

4.　Schäferhans, J.; Gómez-Quero, S.; Aneeva, D.V.; Rothenberg, G. Novel and effective copper-aluminum propane dehydrogenation catalysts. *Chem.-Eur. J.* **2011**, *17*, 12254–12256. [CrossRef] [PubMed]

5.　Beckers, J.; Rothenberg, G. Sustainable selective oxidations using ceria-based materials. *Green Chem.* **2010**, *12*, 939–948. [CrossRef]

6.　Hu, B.; Bean Getsoian, A.; Schweitzer, N.M.; Das, U.; Kim, H.; Niklas, J.; Poluektov, O.; Curtiss, L.A.; Stair, P.C.; Miller, J.T.; et al. Selective propane dehydrogenation with single-site CoII on SiO_2 by a non-redox mechanism. *J. Catal.* **2015**, *322*, 24–37. [CrossRef]

7.　Pakhomov, N.A. Reversible and Irreversible Deactivation of Supported Bimetallic Catalysts for the Dehydrogenation of Lower Paraffins. *Kinet. Catal.* **2001**, *42*, 334–343. [CrossRef]

8.　De Miguel, S.; Castro, A.; Scelza, O.; Fierro, J.L.G.; Soria, J. FTIR and XPS study of supported PtSn catalysts used for light paraffins dehydrogenation. *Catal. Lett.* **1996**, *36*, 201–206. [CrossRef]

9.   Jablonski, E.L.; Castro, A.A.; Scelza, O.A.; de Miguel, S.R. Effect of Ga addition to Pt/Al_2O_3 on the activity, selectivity and deactivation in the propane dehydrogenation. *Appl. Catal. A* **1999**, *183*, 189–198. [CrossRef]

10.   Homs, N.; Llorca, J.; Riera, M.; Jolis, J.; Fierro, J.G.; Sales, J.; de la Piscina, P.R. Silica-supported PtSn alloy doped with Ga, In or, Tl: Characterization and catalytic behavior in n-hexane dehydrogenation. *J. Mol. Catal. A Chem.* **2003**, *200*, 251–259. [CrossRef]

11.   Chen, M.; Xu, J.; Cao, Y.; He, H.; Fan, K.; Zhuang, J. Dehydrogenation of propane over In_2O_3-Al_2O_3 mixed oxide in the presence of carbon dioxide. *J. Catal.* **2010**, *272*, 101–108. [CrossRef]

12.   Hoang, D.L.; Farrage, S.A.F.; Radnik, J.; Pohl, M.M.; Schneider, M.; Lieske, H.; Martin, A. A comparative study of zirconia and alumina supported Pt and Pt–Sn catalysts used for dehydrocyclization of *n*-octane. *Appl. Catal. A* **2007**, *333*, 67–77. [CrossRef]

13.   Liu, Y.; Xia, C.; Wang, Q.; Zhang, L.; Huang, A.; Ke, M.; Song, Z. Direct dehydrogenation of isobutane to isobutene over Zn-doped ZrO_2 metal oxide heterogeneous catalysts. *Catal. Sci. Technol.* **2018**, *8*, 4916–4924. [CrossRef]

14.   Azzam, K.G.; Jacobs, G.; Shafer, W.D.; Davis, B.H. Dehydrogenation of propane over Pt/KL catalyst: Investigating the role of L-zeolite structure on catalyst performance using isotope labeling. *Appl. Catal. A* **2010**, *390*, 264–270. [CrossRef]

15.   Sun, P.; Siddiqi, G.; Vining, W.C.; Chi, M.; Bell, A.T. Novel Pt/Mg(In)(Al)O catalysts for ethane and propane dehydrogenation. *J. Catal.* **2011**, *282*, 165–174. [CrossRef]

16.   Li, Y.; Li, J.; Yang, X.; Wang, X.; Xu, Y.; Zhang, L. Preparation of CeO_2-Modified Mg(Al)O-Supported Pt–Cu Alloy Catalysts Derived from Hydrotalcite-Like Precursors and Their Catalytic Behavior for Direct Dehydrogenation of Propane. *Trans. Tianjin Univ.* **2019**, *25*, 169–184. [CrossRef]

17.   Zhu, Y.; An, Z.; Song, H.; Xiang, X.; Yan, W.; He, J. Lattice-Confined Sn (IV/II) Stabilizing Raft-Like Pt Clusters: High Selectivity and Durability in Propane Dehydrogenation. *Acs Catal.* **2017**, *7*, 6973–6978. [CrossRef]

18.   Gao, S.; Lu, T.; Li, S.; Zhong, H. The mechanism on the pH value influencing the property of glutamic acid/layered double hydroxide compounds. *Colloids Surf. A* **2009**, *351*, 26–29. [CrossRef]

19.   Xia, K.; Lang, W.; Li, P.; Long, L.; Yan, X.; Guo, Y. The influences of MgAl molar ratio on the properties of PtInMg(Al)O-x catalysts for propane dehydrogenation reaction. *Chem. Eng. J.* **2016**, *284*, 1068–1079. [CrossRef]

20.   Mascolo, G.; Mascolo, M.C. On the synthesis of layered double hydroxides (LDHs) by reconstruction method based on the "memory effect". *Micropor. Mesopor. Mater.* **2015**, *214*, 246–248. [CrossRef]

21.   Xia, K.; Lang, W.; Li, P.; Yan, X.; Guo, Y. The properties and catalytic performance of PtIn/Mg(Al)O catalysts for the propane dehydrogenation reaction: Effects of pH value in preparing Mg(Al)O supports by the co-precipitation method. *J. Catal.* **2016**, *338*, 104–114. [CrossRef]

22.   Li, J.; Zhang, M.; Song, Z.; Liu, S.; Wang, J.; Zhang, L. Hierarchical PtIn/Mg(Al)O Derived from Reconstructed PtIn-hydrotalcite-like Compounds for Highly Efficient Propane Dehydrogenation. *Catalysts* **2019**, *9*, 767. [CrossRef]

23.   Gao, Z.; Sasaki, K.; Qiu, X. Structural Memory Effect of Mg–Al and Zn-Al layered Double Hydroxides in the Presence of Different Natural Humic Acids: Process and Mechanism. *Langmuir* **2018**, *34*, 5386–5395. [CrossRef] [PubMed]

24.   Ping, J.; Wang, Y.; Lu, Q.; Chen, B.; Chen, J.; Huang, Y.; Ma, Q.; Tan, C.; Yang, J.; Cao, X.; et al. Self-Assembly of Single-Layer CoAl-Layered Double Hydroxide Nanosheets on 3D Graphene Network Used as Highly Efficient Electrocatalyst for Oxygen Evolution Reaction. *Adv. Mater.* **2016**, *28*, 7640–7645. [CrossRef]

25.   Yang, S.; Zhang, Z.; Zhou, J.; Sui, Z.; Zhou, X. Hierarchical NiCo LDH-rGO/Ni Foam Composite as Electrode Material for High-Performance Supercapacitors. *Trans. Tianjin Univ.* **2019**, *25*, 266–275. [CrossRef]

26.   Jiang, J.; Zhu, J.; Ding, R.; Li, Y.; Wu, F.; Liu, J.; Huang, X. Co-Fe layered double hydroxide nanowall array grown from an alloy substrate and its calcined product as a composite anode for lithium-ion batteries. *J. Mater. Chem.* **2011**, *21*, 15969. [CrossRef]

27.   Zhu, Y.; An, Z.; He, J. Single-atom and small-cluster Pt induced by Sn (IV) sites confined in an LDH lattice for catalytic reforming. *J. Catal.* **2016**, *341*, 44–54. [CrossRef]

28.   Chen, X.; Chen, X.; Wang, L.; Wang, L.; Qin, H.; Qin, H.; Yang, Z.; Yang, Z. Fabrication and electrochemical performance of flower-like ZnAl LDH/SnO_2 composites for zinc-nickel secondary batteries. *Ionics* **2019**, *25*, 1715–1724. [CrossRef]

29. Wang, F.; Liu, M.; Zhang, X.; Lv, G.; Sun, M. In Situ Growth of 3D Hierarchical ZnO@Ni$_x$Co$_{1-x}$(OH)$_y$ Core/Shell Nanowire/Nanosheet Arrays on Ni Foam for High-Performance Aqueous Hybrid Supercapacitors. *Trans. Tianjin Univ.* **2018**, *24*, 201–211. [CrossRef]

30. Shen, L.; Xia, K.; Lang, W.; Chu, L.; Yan, X.; Guo, Y. The effects of calcination temperature of support on PtIn/Mg(Al)O catalysts for propane dehydrogenation reaction. *Chem. Eng. J.* **2017**, *324*, 336–346. [CrossRef]

31. Yang, Y.; Fan, G.; Li, F. Synthesis of novel marigold-like carbonate-type Mg-Al layered double hydroxide micro-nanostructures via a two-step intercalation route. *Mater. Lett.* **2014**, *116*, 203–205. [CrossRef]

32. Filez, M.; Redekop, E.A.; Poelman, H.; Galvita, V.V.; Meledina, M.; Turner, S.; Van Tendeloo, G.; Detavernier, C.; Marin, G.B. One-pot synthesis of Pt catalysts based on layered double hydroxides: An application in propane dehydrogenation. *Catal. Sci. Technol.* **2016**, *6*, 1863–1869. [CrossRef]

33. Stepanova, L.N.; Belskaya, O.B.; Likholobov, V.A. Effect of the Nature of the Active-Component Precursor on the Properties of Pt/MgAlO$_x$ Catalysts in Propane and *n*-Decane Dehydrogenation. *Kinet. Catal.* **2017**, *4*, 400–409. [CrossRef]

34. Wu, J.; Peng, Z.; Sun, P.; Bell, A.T. n-Butane dehydrogenation over Pt/Mg(In)(Al)O. *Appl. Catal. A* **2014**, *470*, 208–214. [CrossRef]

35. Larsson, M.; Hultén, M.; Blekkan, E.A.; Andersson, B. The Effect of Reaction Conditions and Time on Stream on the Coke Formed during Propane Dehydrogenation. *J. Catal.* **1996**, *164*, 44–53. [CrossRef]

36. Airaksinen, S.M.K.; Krause, A.O.I.; Sainio, J.; Lahtinen, J.; Chao, K.; Ares, M.O.G.R. Reduction of chromia/alumina catalyst monitored by DRIFTS-mass spectrometry and TPR-Raman spectroscopy. *Phys. Chem. Chem. Phys.* **2003**, *20*, 4371–4377. [CrossRef]

37. Hakuli, A.; Kytokivi, A.; Krause, A.O.I.; Suntola, T. Initial Activity of Reduced Chromia/Alumina Catalyst in *n*-Butane Dehydrogenation Monitored by On-Line FT-IR Gas Analysis. *J. Catal.* **1996**, *161*, 393–400. [CrossRef]

38. Galvita, V.; Siddiqi, G.; Sun, P.; Bell, A.T. Ethane dehydrogenation on Pt/Mg(Al)O and PtSn/Mg(Al)O catalysts. *J. Catal.* **2010**, *271*, 209–219. [CrossRef]

39. Santhosh Kumar, M.; Chen, D.; Walmsley, J.C.; Holmen, A. Dehydrogenation of propane over Pt-SBA-15: Effect of Pt particle size. *Catal. Commun.* **2008**, *9*, 747–750. [CrossRef]

40. Chen, X.; Ge, M.; Li, Y.; Liu, Y.; Wang, J.; Zhang, L. Fabrication of highly dispersed Pt-based catalysts on γ-Al$_2$O$_3$ supported perovskite Nano islands: High durability and tolerance to coke deposition in propane dehydrogenation. *Appl. Surf. Sci.* **2019**, *490*, 611–621. [CrossRef]

41. Xia, K.; Lang, W.; Li, P.; Yan, X.; Guo, Y. Analysis of the catalytic activity induction and deactivation of PtIn/Mg(Al)O catalysts for propane dehydrogenation reaction. *Rsc Adv.* **2015**, *5*, 64689–64695. [CrossRef]

42. Wang, T.; Jiang, F.; Liu, G.; Zeng, L.; Zhao, Z.J.; Gong, J. Effects of Ga doping on Pt/CeO$_2$-Al$_2$O$_3$ catalysts for propane dehydrogenation. *Aiche J.* **2016**, *62*, 4365–4376. [CrossRef]

43. Yu, J.; Wang, R.; Ren, S.; Sun, X.; Chen, C.; Ge, Q.; Fang, W.; Zhang, J.; Xu, H.; Su, D.S. The Unique Role of CaO in Stabilizing the Pt/Al$_2$O$_3$Catalyst for the Dehydrogenation of Cyclohexane. *Chemcatchem* **2012**, *4*, 1376–1381. [CrossRef]

44. Mitchell, P.C.H.; Wass, S.A. Propane dehydrogenation over molybdenum hydrotalcite catalysts. *Appl. Catal. A* **2002**, *225*, 153–165. [CrossRef]

45. Mokhtar, M.; Inayat, A.; Ofili, J.; Schwieger, W. Thermal decomposition, gas phase hydration and liquid phase reconstruction in the system Mg/Al hydrotalcite/mixed oxide: A comparative study. *Appl. Clay Sci.* **2010**, *50*, 176–181. [CrossRef]

46. Pérez-Ramírez, J.; Abelló, S.; van der Pers, N.M. Memory Effect of Activated Mg-Al Hydrotalcite: In Situ XRD Studies during Decomposition and Gas-Phase Reconstruction. *Chem.-Eur. J.* **2007**, *13*, 870–878. [CrossRef]

47. Airaksinen, S.M.K.; Harlin, M.E.; Krause, A.O.I. Kinetic Modeling of Dehydrogenation of Isobutane on Chromia/Alumina Catalyst. *Ind. Eng. Chem. Res.* **2002**, *41*, 5619–5626. [CrossRef]

48. Derossi, S.; Ferraris, G.; Fremiotti, S.; Garrone, E.; Ghiotti, G.; Campa, M.C.; Indovina, V. Propane Dehydrogenation on Chromia/Silica and Chromia/Alumina catalysts. *J. Catal.* **1994**, *148*, 36–46. [CrossRef]

49. Prinetto, F.; Ghiotti, G.; Durand, R.; Tichit, D. Investigation of Acid−Base Properties of Catalysts Obtained from Layered Double Hydroxides. *J. Phys. Chem. B* **2000**, *104*, 11117–11126. [CrossRef]

50. Mounfield, W.P.; Claure, M.T.; Agrawal, P.K.; Jones, C.W.; Walton, K.S. Synergistic Effect of Mixed Oxide on the Adsorption of Ammonia with Metal-Organic Frameworks. *Ind. Eng. Chem. Res.* **2016**, *22*, 6492–6500. [CrossRef]

51. Rao, K.K.; Gravelle, M.; Valente, J.S.; Figueras, F. Activation of Mg-Al Hydrotalcite Catalysts for Aldol Condensation Reactions. *J. Catal.* **1998**, *173*, 115–121. [CrossRef]

52. Liu, G.; Zhao, Z.; Wu, T.; Zeng, L.; Gong, J. Nature of the Active Sites of VO_x/Al_2O_3 Catalysts for Propane Dehydrogenation. *Acs Catal.* **2016**, *6*, 5207–5214. [CrossRef]

53. Han, Z.; Li, S.; Jiang, F.; Wang, T.; Ma, X.; Gong, J. Propane dehydrogenation over Pt-Cu bimetallic catalysts: The nature of coke deposition and the role of copper. *Nanoscale* **2014**, *6*, 1–18. [CrossRef] [PubMed]